THE JOURNAL OF PHYSICAL CHEMISTRY B
A JOURNAL OF THE AMERICAN CHEMICAL SOCIETY

pubs.acs.org/JPCB

Article

Exploring the Interplay between Disordered and Ordered Oligomer Channels on the Aggregation Energy Landscapes of α-Synuclein

Published as part of The Journal of Physical Chemistry virtual special issue "Jose Onuchic Festschrift".

Xun Chen, Mingchen Chen, and Peter G. Wolynes*

Cite This: https://doi.org/10.1021/acs.jpcb.2c03676

Read Online

ACCESS | Metrics & More | Article Recommendations | Supporting Information

ABSTRACT: The abnormal aggregation of α-synulcein is associated with multiple neurodegenerative diseases such as Parkinson's disease. The hydrophobic non-amyloid component (NAC) region of α-synuclein comprises the core of the fibril in vitro and in vivo. In this work, we study the aggregation landscape of the hydrophobic NAC region of α-synuclein using a transferrable coarse-grained force field, the associative memory water-mediated structure, and energy model (AWSEM). Using structural similarity, we can group metastable states on the free energy landscape of aggregation into three types of oligomers: disordered oligomers, prefibrillar oligomers with disordered tips, and ordered prefibrillar oligomers. The prefibrillar oligomers with disordered tips have more in-register parallel β strands than do the fully disordered oligomers but have fewer in-register parallel β strands than the ordered prefibrillar oligomers. Along with the ordered prefibrillar species, the disordered oligomeric states dominate at small oligomer sizes while the prefibrillar species with disordered tips thermodynamically dominate with the growth of oligomers. The topology of the aggregation landscape and observations in simulations suggest there is backtracking between ordered prefibrillar oligomers and other kinds of oligomers as the aggregation proceeds. The significant structural differences between the ordered prefibrillar oligomers and the disordered oligomers support the idea that the growth of these two kinds of oligomers involves kinetically independent parallel pathways. In contrast, the overall structural similarity between the fully ordered prefibrillar oligomers and the prefibrillar oligomers with disordered tips implies that two channels can interconvert on slower time scales. We also evaluate the effects of phosphorylation on the aggregation free energy landscape using statistical mechanical perturbation theory.

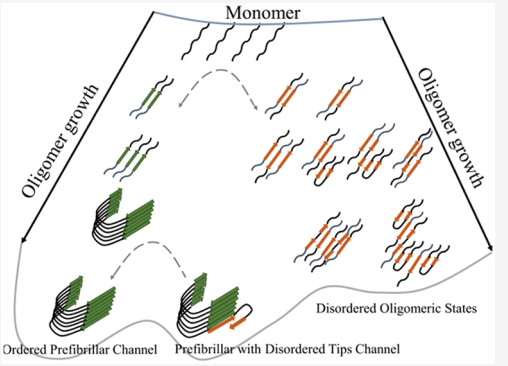

1. INTRODUCTION

Many neurodegenerative diseases are synucleinopathies which involve the abnormal aggregation of α-synuclein. These include Parkinson's disease (PD), dementia with Lewy bodies disease, and multiple systems atrophy (MSA).[1,2] In Parkinson's diseases, several lines of evidence have highlighted the critical role of α-synuclein as the main misfolded species that is a constituent of neurites and Lewy bodies.[3] Nevertheless, the relative toxicity of the different α-synuclein species is still unclear. Many researchers favor the idea that the toxicity of α-synuclein to neurons mainly comes from the oligomeric species rather than fibrillar species.[4] In this paper, we explore the kinetic and thermodynamic interplay between the different species of oligomers of different sizes using a realistic computational model that has already succeeded in characterizing aspects of the aggregation processes of Huntingtin proteins,[5] Aβ peptides,[6] polyglutamine repeats,[7] and tau protein.[8]

The synuclein family of proteins, abundant in the brain, includes α-synuclein, β-synuclein, and γ-synuclein.[9] These three isoforms mutually possess 55−62% similarity in sequence and range from 127 to 140 amino acids in length.[10] While α-synuclein assembles into filaments, neither β-synuclein nor γ-synuclein prefers to assemble into filaments.[9] α-Synuclein is considered to be an intrinsically disordered protein (IDP) and consists of three domains: an acidic C-terminal domain which stabilizes its interaction with other proteins,[11] a hydrophobic non-amyloid component (NAC) region which is prone to aggregate into fibrils,[11] and an amphipathic repeat region which forms a stable helical structure in association with lipid micelles.[12]

While α-synuclein is an intrinsically disordered protein (IDP) in its monomeric form, it aggregates into several different polymorphs in vitro.[13] The availability of the

Received: May 28, 2022
Revised: June 24, 2022

atomistic structure of α-synuclein fibrils provides a basis to understand the mechanisms underlying its aggregation and may help to develop therapies. Guerrero-Ferreira and co-workers have recently experimentally determined the fibril structure of α-synuclein by cryo-EM.[14] The structure of the α-synuclein fibril determined in this way includes the hydrophobic NAC region as the fibrillar core which forms multiple in-register parallel β-strands much as seen in amyloids. Except for the hydrophobic NAC region, the structure suggests the other residues are disordered surrounding this core and serve as a "fuzzy coat", similar to what is seen for tau protein.[14,15]

In vivo, the aggregation process of α-synuclein is quite complex, being influenced by several different modifications such as mutations at the amphipathic repeat region, nitration at tyrosine residues, ubiquitination, phosphorylation, C-terminal truncation, and modification by dopamine.[16−19] These modifications affect the binding affinity of deposited α-synuclein with membrane lipid[20] and alter the stability of its different oligomeric states and the stability of its insoluble fibrils.[18−20] In Parkinson's disease (PD), most of the α-synuclein species are phosphorylated.[21] Although some kinases regulating phosphorylation in vitro have been identified, the specific kinases involved and the mechanism of phosphorylation are still unclear in vivo.[22] The most favorable phosphorylated sites include S87, Y125, S129, Y133, and Y136 of α-synuclein.[18] Among all the phosphorylated sites of α-synuclein identified in experiments, the hydrophobic non-amyloid component (NAC) region only possesses one phosphorylated site, S87, implying this site may have a essential role in aggregation.[19] Furthermore, S87 is absent in the α-synucleins of mouse and of rat, suggesting that the behaviors of S87, under phosphorylation, may distinguish the differences seen between α-synuclein aggregation in humans and in mice and rats.[19] Motivated by these observations, we investigate the effects of phosphorylating S87 on the aggregation free energy landscape using statistical mechanical perturbation theory in this work.

The molecular dynamics simulation of protein aggregation still remains challenging because of the large size of the aggregation system which must involve multiple copies of a sizable protein. To meet this computational challenge, we have used a coarse-grained, transferable, and realistic force field to survey the aggregation landscapes of several proteins that form amyloids involved in neurodegenerative diseases. Previously, we have successfully used a specific coarse-grained model, the associative memory water-mediated structure, and energy model (AWSEM) which has been tested in folded protein structural prediction to study the aggregation process of Aβ[6] and tau protein.[8]

In the present work, we use the AWSEM force field to study the aggregation free energy landscape of α-synuclein. Similar to what we found for tau protein, we find both disordered oligomers and ordered prefibrillar oligomers in the aggregation landscape. Furthermore, the backtracking between these two classes of oligomers and the growth of these oligomers were also observed in the simulations. Besides these two classes, another distinctive structured class, the prefibrillar species with disordered tips, was found in the landscape when the oligomer size is sufficiently large. We further explore the differences between the prefibrillar species with and without disordered tips and their competition with the growth of fully disordered oligomers. Considering the structural similarity between prefibrillar oligomers with disordered tips and fully ordered prefibillar oligomers, we propose that generally there is a backtracking mechanism between the two channels, which may be quite slow.

2. METHODS

2.1. AWSEM Force Field. The Associative memory, Water-mediated, Structure Energy Model (AWSEM) is a predictive coarsed-grained protein force field where the parameters of force field have been optimized by using a machine learning strategy based on the energy landscape theory and the available native structures of proteins from the PDB database.[23] The details of the construction of AWSEM and previous examples employing it for protein aggregation simulations can be found in Davtyan et al.[23] and Chen et al.[7] In those works, readers will also find the procedures by which we correct the free energy profile for the varying concentration of free monomers using physical cluster theory from statistical mechanics and use this theory also to compute the free energy landscape based on AWSEM at various concentrations of monomer.[6,7] The AWSEM force field has already proved itself useful in protein structure prediction,[24,24] protein−protein interaction,[25] protein−DNA interaction,[26] and other examples of aggregation,.[5−8]

2.2. Order Parameters Using in Umbrella Sampling. The similarity measurement $Q_w^{\alpha\beta}$ provides a useful way to measure the similarity between a given structure α and another structure β.[27] $Q_w^{\alpha\beta}$ is defined through the relation

$$Q_w^{\alpha\beta} = \frac{2}{(N-2)(N-3)} \sum_{j-i>2} \exp[-(r_{ij}^{\alpha} - r_{ij}^{\beta})^2/2\sigma_{ij}^2],$$
$$\sigma_{ij} = |j-i|^{0.15} \quad (1)$$

Here N is the total number of residues in the structure. r_{ij}^{α} is the distance between the Cα atoms of residue i and residue j in the structure α, and r_{ij}^{β} is the distance between the Cα atoms of the corresponding residues in the structure β. σ_{ij} is a sequence separation-dependent well width.[7]

To enhance the sampling of organized structures for aggregation to be used in free energy calculation, we employed umbrella sampling with a harmonic potential in Q_w with respect to a fibril structure (PDB ID: 6H6B) within a range of reference values:

$$V_{Q\text{-bias}} = \frac{1}{2} k_{Q\text{-bias}} (Q - Q_0)^2 \quad (2)$$

with $k_{Q\text{-bias}}$ = 1200 kcal/mol. The reference values for Q_0 are equally spaced from 0 to 0.998 with a step size of 0.002. We used the weighted histogram analysis method (WHAM) to collect data from all windows to construct full free energy landscapes.

Another set of umbrella simulations was performed by using another reaction coordinate Q_{diff} defined as

$$Q_{diff} = \frac{q - q_1}{q_1 - q_2} \quad (3)$$

$$q(r_{ij}) = \frac{1}{(N-2)(N-3)} \sum_{j>i+2} [e^{-(r_{ij}-r_{ij}^{N1})/2\sigma_{ij}^2} - e^{-(r_{ij}-r_{ij}^{N2})/2\sigma_{ij}^2}] \quad (4)$$

The umbrella sampling using Q_{diff} allows us to sample efficiently the structures between the fully ordered prefibrillar structure and the prefibrillar structures with disordered tips. N

https://doi.org/10.1021/acs.jpcb.2c03676
J. Phys. Chem. B XXXX, XXX, XXX−XXX

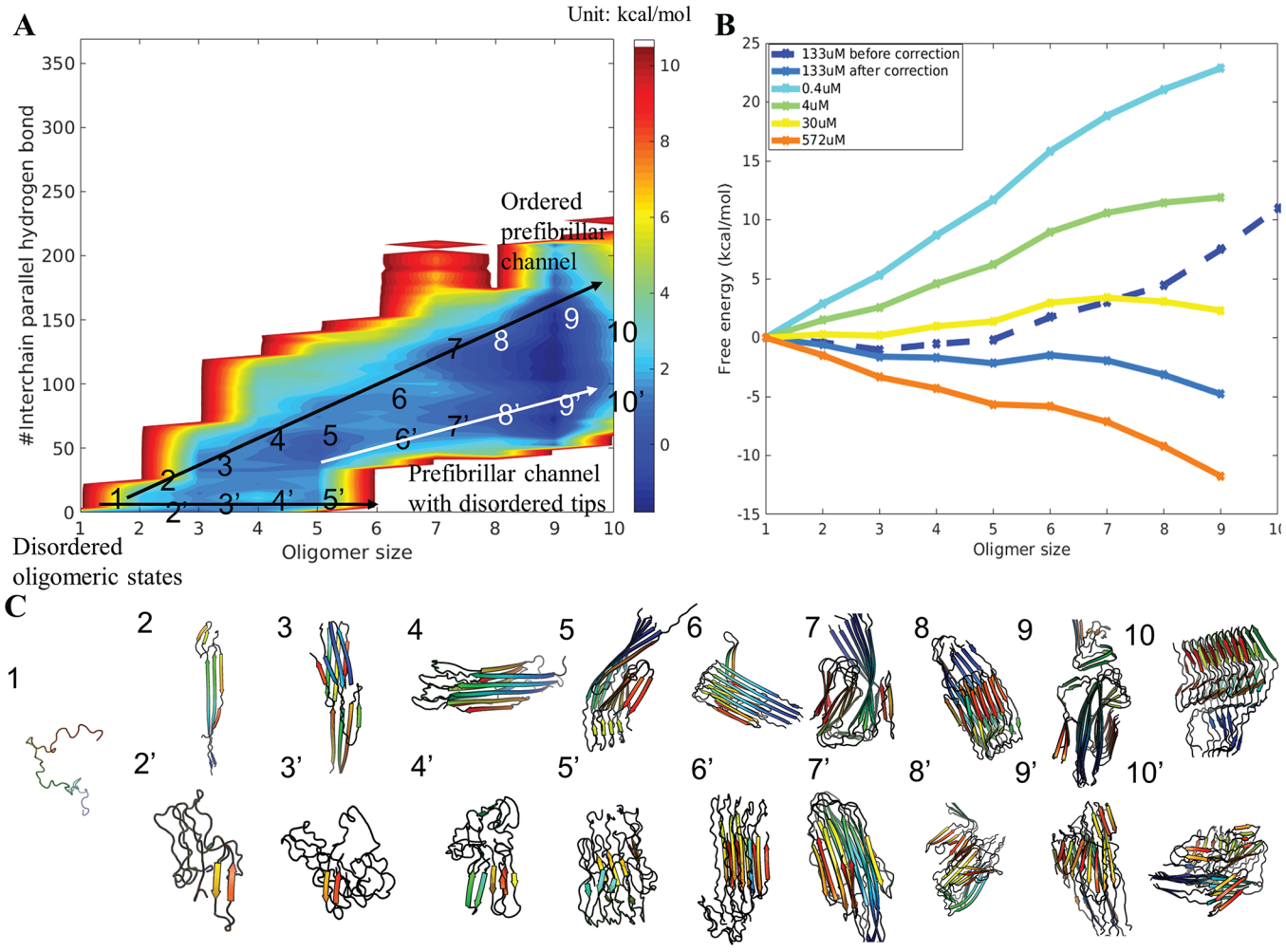

Figure 1. Grand canonical free energy profiles for α-synuclein at a temperature of 300 K. (A) The 2D free energy surface at the concentration of 133 μM is plotted by using the oligomer size and the number of interchain parallel hydrogen bonds as coordinates. The number of interchain parallel hydrogen bonds measures the amount of fibril-like β-sheet formed between different chains. The basins for different oligomeric states are labeled. Free energies are shown in rainbow colors (in units of kcal/mol). (B) The grand canonical free energy for different oligomers after finite-size correction under different concentration shows the saturation value of the concentration of free monomers. (C) Representative structures of the different species in each basin are shown: each monomer is colored with a rainbow spectrum from blue to red, C-terminus to N-terminus.

and σ_{ij} are defined as before. $q_1 = q(r_{ij}^{N_1})$ and $q_2 = q(r_{ij}^{N_2})$ where the prefibrillar structure with disordered tips and the ordered prefibrillar structure are labeled as structures 1 and 2.[28] As in eq 3, $k_{Q\text{-bias}}$ = 3000 kcal/mol, and Q_0, the biasing center values, range from 0.02 to 0.98 with equal space 0.02.

2.3. Simulation Details. In this study, all the umbrella sampling simulations were performed by using the LAMMPS software (the large-scale atomic/molecular massively parallel simulator). One set of umbrella simulations was run at 300 K for 6 million steps (corresponding to roughly 30 μs in lab time). The initial configuration used in these simulations consists of ten free monomers randomly distributed in a cubic box with periodic boundary conditions (133 μM). Another set of umbrella simulations was performed at 300 K for 4 million steps (corresponding to 20 μs in lab time). The initial configurations for these simulations consisted of one octamer 100 Å away from one free monomer in a cubic box of 500 Å with periodic boundary conditions. Under the umbrella sampling conditions, these times are enough to ensure sampling convergence for the aggregation free energy profile. We inferred the free energy landscapes using physical cluster theory from statistical mechanics theory for a range of monomer concentrations. The procedure for dong this can be found in Chen et al.[7] and Zheng et al.[6]

2.4. Quantification of Phosphorylation Effects on the Aggregation Landscapes Using Free Energy Perturbation. The AMH model, the predecessor of the AWSEM force field, was used a long while ago to study the thermodynamic effects of phosphorylation on free energy profiles.[29] This model treats the phosphorylated serines and threonines residues as "super-charged" glutamic acid residues.[30] Because the pK_as of the phosphorylated serine and threonine residues are around 7 in the experiment, we have adopted the same strategy as was done previously for the AMH model. Because only Ser87 of the hydrophobic NAC (non-amyloid component) region in simulations is identified as being an accessible phosphorylation site in experiment,[19] we phosphorylated the Ser87 using perturbation analysis as shown in Figure 6A. To quantify the effects of phosphorylation on the aggregation landscape, we applied the free energy perturbation to an unphosphorylated protein aggregation simulation previously carried out. Then we recalculated the energies of the sampled

https://doi.org/10.1021/acs.jpcb.2c03676
J. Phys. Chem. B XXXX, XXX, XXX−XXX

structures with the phosphorylated AWSEM force field to evaluate the energy changes (ΔE) as averages:

$$\Delta E = \langle E_{\text{phosphorylated}} - E_{\text{unphosphorylated}} \rangle_{\text{av}} \quad (5)$$

The free energy changes (ΔF) are well approximated as the energy changes (ΔE).[6]

2.5. Localized Frustration Analysis and Cluster Analysis. Generally, we quantify structural energetic frustration in proteins through the localized energetic frustration, which is computed by first evaluating the energy of a protein in its native states and then comparing this energy to the range of energies of decoy states created by locally shuffling residues using as a starting point a high-resolution structure of the protein along with a sufficiently accurate energy function.[31,32] Here we used the frustration index to analyze the energetic fitness of α-synulcein oligomers compared with their possible decoys.[31] On the basis of the frustration index, contacts within the oligomers can be classified as being highly frustrated, neutrally frustrated, or minimally frustrated.[33] As in previous studies, contacts having a frustration index above 0.78 are identified as minimally frustrated interactions, while contacts having a frustration index below −1.0 are identified as highly frustrated interactions.[31,34]

Representative structures of each oligomer formed in the simulations were clustered by using a hierarchical algorithm with a "centroid" linkage scheme.[35] We used mutual Q to build the linkage matrix to obtain the clusters. The mutual $Q^{\alpha\beta}$ between structure α and structure β is symmetric in cluster map as defined in eq 2. The clusters of structures are identified by having their mutual Q values above 0.45. On the basis of the N-mers from the simulation, we can also build the corresponding $(N-1)$-mer's structure by removing a single chain at the end of the N-mer structure. Then we can recalculate the mutual Q and plot the cluster map using the same order of x, y-axes as the cluster map of the N-mer for comparison.

2.6. Data Availability. The input files, data from simulations and analyses, and analysis codes in this work are deposited in GitHub: https://github.com/further-explore/alpha-synuclein.

3. RESULTS

3.1. Aggregation Landscapes of α-Synuclein. We have studied the aggregation landscape of the hydrophobic NAC region of α-synuclein, which is found in the fibrils derived from Parkinson's disease (PD) patients. The solved structure for the fibril by Guerrero and co-workers has a fibrillar core of 58 residues (residues 38−95 of 140 residues).[14] The fibrillar core is buried in a fuzzy coat formed by other residues. Guerrero and co-workers have determined that the fibril structure is constructed from two protofilaments, akin to the symmetry characteristic of the paired helical filaments of tau.[14]

We constructed the free energy landscape of α-synuclein aggregation for ten monomers in a simulation box under 133 μM using a single protofilament as a template for umbrella sampling. We performed the umbrella sampling simulation using the $Q_{ij}^{\alpha\beta}$ between the sampled structure and the experimentally determined structure (PDBID: 6H6B) as the biasing coordinate to build free energy profiles. Then, as is shown in Figure 1A, we projected the free energy onto a two-dimensional surface using as one coordinate the number of intermolecular parallel hydrogen bonds in oligomers (quantifying the formation of fibrillar-like β strand) and as the other coordinate the corresponding oligomer size. Representative oligomeric structures for each basin are labeled in Figure 1A. Besides monomeric species (structure **1** in Figure 1C), when the oligomer size is smaller than **6**, two kinds of species are found: (1) disordered oligomers with fewer interchain parallel hydrogen bonds; (2) ordered prefibrillar oligomers with a large number of interchain parallel hydrogen bonds. These distinct species suggest quasi-independent growth of amorphous oligomeric states and the ordered prefibrillar states when the oligomer size is small, paralleling the mechanism proposed by Chen et al. for tau aggregation.[8] When the oligomer size increases further, the ordered prefibrillar species behave as the ordered oligomeric states do at the small oligomer size. In addition, however, we find another species with many interchain parallel hydrogen bonds. In this class, the number of interchain hydrogen bonds is more than for the disordered species but is fewer than for the fully ordered prefibrillar species, which are also found in Aβ aggregation.[36] These species, which we call prefibrillar oligomers with disordered tips, are dominated by fibril-like β sheet chains with the addition of a few β hairpin chains at the ends. The existence of two kinds of species, the fully ordered prefibrillar oligomers and the prefibrillar oligomers with disordered tips, agrees with FRET experiments which suggest there are two classes of species when the oligomer size is larger than **5**.[37,38] The disordered species of small oligomer size will aggregate into a macroscopic amorphous phase downhill in free energy at or above the simulated concentration of 133 μM. Further growth of the amorphous oligomers is not, however, the most thermodynamically favored in comparison with the growth of ordered prefibrillar species and prefibrillar species with disordered tips (Figure 1A). Moreover, the ordered prefibrillar species and prefibrillar species with disordered tips will continue to grow to high-order species as seemingly distinct channels. At the simulation concentration of 133 μM, the barriers for interconversion between the amorphous oligomers and the ordered prefibrillar oligomers are larger than the barriers for the steps in the growth of the two kinds of prefibrillar oligomers, which suggests two kinetically independent oligomerization channels during aggregation: the ordered prefibrillar species will grow to the amyloid fiber, but the disordered species finally will reach a macroscopic amorphous phase. It is hard to discriminate the barriers between the ordered prefibrillar channel and prefibrillar channel with disordered tips and the barriers for the growth of the two channels on this two-dimensional free energy surface (Figure 1A), which we will discuss later.

The store of monomers is depleted as the oligomer grows in our simulations with a finite number of monomers in a finite box. We have adopted the Reiss and Bowles theory[39] as in our previous work[6] to correct for this finite size effect to construct a one-dimensional grand canonical free energy profile. The free energy after correction is downhill at the simulation concentration (133 μM) (the solid blue lines in Figure 1B), which means that the growth of oligomers is favorable at this concentration. The free energy profile can be extrapolated to different concentrations by considering how the chemical potential changes with concentration, which can then be used to evaluate the solubility limits and critical nucleus size.[6] The solubility is assessed as the lowest concentration, where the grand canonical free energy profile becomes downhill at the largest oligomer size that is sampled.[7] From our calculations,

https://doi.org/10.1021/acs.jpcb.2c03676
J. Phys. Chem. B XXXX, XXX, XXX−XXX

the solubility of the α-synuclein region (residues 38−95) is determined to be around 4 μM, which agrees well with the experimental value 0.4 2.7 μM.[37,40] The critical nucleus size can be estimated as the size of the oligomer corresponding to the peak of the grand canonical free energy profile.[7] The critical nucleus size turns out to be around 2−3 in our calculation, in agreement with experimental determinations of the critical nucleus size.[37,41] As shown in Figure S8A,B, the free energy profiles become completely downhill at a concentration of 572 μM, which can be called "supercritical". The prefibrillar species and the prefibrillar species with disordered tips become dominant, suggesting spontaneous fibril formation above supercritical concentration.[42,43]

We did not observe any examples of a direct transition between the disordered oligomers and their corresponding ordered prefibrillar species during the simulations. Nevertheless, the dissociation and reassociation of the disordered and ordered prefibrillar species were often observed when the oligomer size is small. This pattern is the same as we saw for tau aggregation, suggesting there is a kinetic backtracking mechanism. The disordered oligomer cannot directly transit to its ordered prefibrillar counterpart. Instead, it needs to dissociate into monomers and then reassociate to the ordered prefibrillar oligomer. The interconversion between the prefibrillar species with disordered tips and the ordered prefibrillar species will be discussed later.

3.2. Characteristics of the Prefibrillar Oligomers with Disordered Tips in α-Synuclein Aggregation. We have already observed the channel corresponding to fibers with disordered tips in the aggregation free energy profile as shown in Figure 1A. We next explored the characteristics of these structures using frustration analysis. Frustration analysis is a useful tool for understanding structural and functional details based on energy landscape theory.[31] All the sampled structures were quantified by their total frustration levels. Then we constructed a new two-dimensional free energy profile using the number of minimally frustrated interactions and the number of highly frustrated interactions among ten monomers as coordinates. As discussed in the Methods section, a minimally frustrated interaction indicates that this contact should be among the most stable among its alternative structures so that there is no driving force to change this contact in functional motions, while a highly frustrated interaction suggests that this contact is energetically unfavorable which makes it much easier for it to access other alternative structures.[31] Three basins are identified on this free energy landscape in Figure 2: The disordered oligomeric species possess the fewest number of minimally frustrated interactions, which reflects that these species are easiest to change to other kinds of oligomeric species during aggregation. This observation is also consistent with the conclusion that the amorphous oligomeric states are not favorable compared to the ordered prefibrillar states when oligomer size is small, as shown in Figure 1A. In contrast to the fully ordered prefibrillar species, the prefibrillar species with disordered tips have fewer minimally frustrated interactions and more highly frustrated interactions, suggesting that the fully ordered prefibrillar species will be more energetically favorable as the oligomer grows.

The differences between the three classes of oligomers are significant, as shown in Figure 1C. In Figures S1 and S2, we further explored the buildup of these oligomers. Starting from the oligomer structures without monomers, we selected 200

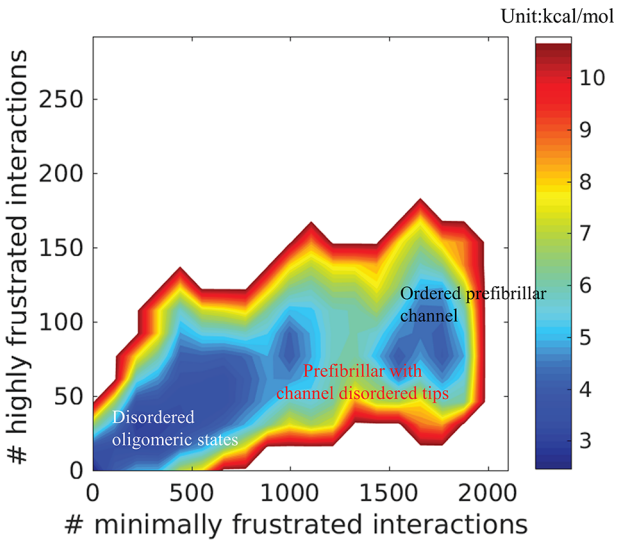

Figure 2. Grand canonical free energy profile for all oligomers of α-synuclein at a temperature of 300 K. The 2D free energy surface at the concentration of 133 μM is plotted by using the number of minimally frustrated interactions and the number of highly frustrated interactions. A minimally frustrated interaction indicates that this interaction between two residues is quite stable, while a highly frustrated interaction indicates that the contact between these two residues is unstable. Free energies are shown in rainbow colors (in units of kcal/mol).

frames with the same step size to build N-mer and $(N-1)$-mer cluster maps from all the sampled structures. In the tetramer cluster maps in Figure S1, three kinds of clusters are found. The mutual Q of disordered tip structures (labeled 1) of $(N-1)$-mer cluster map decreases compared with N-mer cluster map, suggesting the β-hairpin structures of end monomers. In contrast, the mutual Q of amorphous oligomers (labeled 2) increases, and the mutual Q of ordered prefibrillar oligomers (labeled 3) does not change much. Three clusters with the corresponding characteristics are observed in the heptamer cluster maps in Figure S2, also supporting the β-hairpin structure of the end monomers in prefibrillar oligomers with disordered tips.

3.3. Changes in the Prefibrillar Channels during Oligomer Growth. We have already found that prefibrillar oligomers with disordered tips appear in the tetramers and heptamers (Figures S1 and S2). In the aggregation landscape, the amorphous oligomeric states dominate when the oligomer size is smaller than **6**, while the prefibrillar states with disordered tips dominate once the oligomer size is larger than **5** (Figure 1A. Furthermore, we explored the changes in the prefibrillar channels as oligomers grow. In Figure 1, we have constructed the free energy landscapes from trimers to heptamers using the number of interchain parallel hydrogen bonds and the number of interchain antiparallel hydrogen bonds as coordinates. The amorphous oligomeric states possess the fewest interchain parallel hydrogen bonds and the largest amount of interchain antiparallel hydrogen bonds, while the ordered prefibrillar species have the largest amount of interchain parallel hydrogen bonds and the fewest interchain antiparallel hydrogen bonds. The number of interchain parallel hydrogen bonds and the number of interchain antiparallel hydrogen bonds of prefibrillar species with disordered tips are between the corresponding numbers of hydrogen bonds of the amorphous oligomeric species and the ordered prefibrillar

https://doi.org/10.1021/acs.jpcb.2c03676
J. Phys. Chem. B XXXX, XXX, XXX−XXX

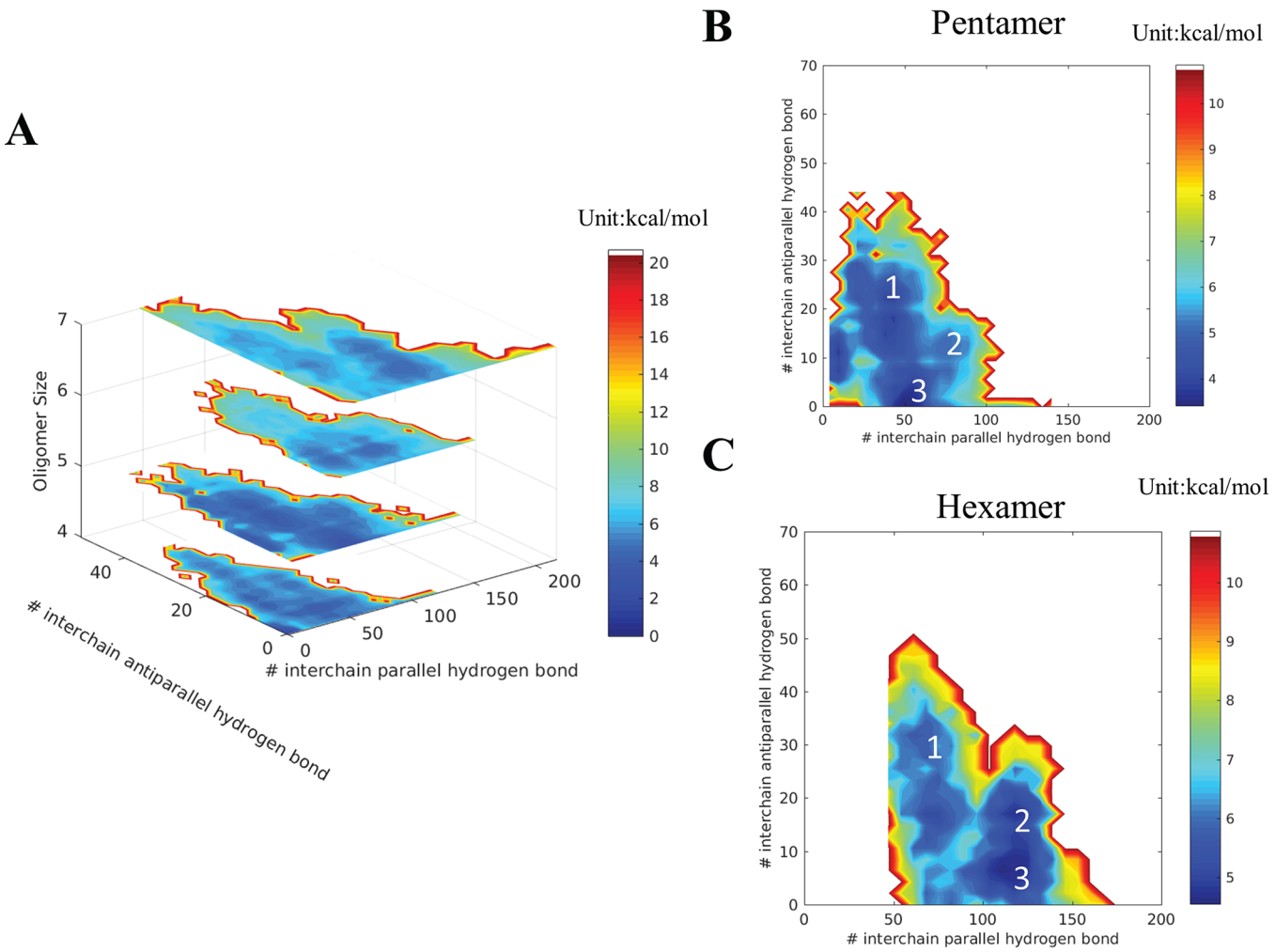

Figure 3. Grand canonical free energy profiles for α-synuclein at a temperature of 300 K. (A) The stacking of 2D free energy profiles of different oligomer sizes at the concentration of 133 μM is plotted by using the number of intermolecular parallel hydrogen bonds and the number of intermolecular antiparallel hydrogen bonds. (B) The 2D free energy profile of the pentamer at the concentration of 133 μM is plotted by using the number of intermolecular parallel hydrogen bonds and the number of intermolecular antiparallel hydrogen bonds. (C) The 2D free energy profile of the hexamer at the concentration of 133 μM is plotted by using the number of intermolecular parallel hydrogen bonds and the number of intermolecular antiparallel hydrogen bonds. These profiles have been corrected for the concentration change. Free energies are shown in rainbow colors (in units of kcal/mol)

species. Compared with the free energy profile of pentamers (Figure 3B), the disordered oligomeric states become less favorable, and the prefibrillar states with disordered tips become more favorable in the free energy profile at the stage of hexamers (Figure 3C). As shown in Figure 3A, the stacked free energy profiles for different sizes indicate that the prefibrillar channel having disordered tips becomes more favorable once the oligomer size increases sufficiently, in consonance with what is seen in Figure 1A. We have also constructed the free energy profiles of different oligomers using as coordinates the number of minimally frustrated interactions and the number of highly frustrated interactions (Figure S3). This profile also supports the same trend in the aggregation process.

To verify the change in relative preference for the two distinct prefibrillar channels as the oligomers grow, we further constructed free energy profiles of the tetramers and heptamers using Q_w of the N-mer and Q_w of the $(N-1)$-mer. The Q_w of the prefibrillar oligomers with disordered tips increases when their end monomer dissociates, while the Q_w of the fully disordered oligomers decreases upon dissociation, and the Q_w of the ordered prefibrillar species does not change much (Figures S1 and S2). Therefore, we see that we can divide the free energy profiles into three regions: (1) a disordered oligomeric states region where Q_w of the N-mer is larger than Q_w of the corresponding $(N-1)$-mer; (2) a corresponding region of prefibrillar oligomers with disordered tips where Q_w of the N-mer is smaller than Q_w of the corresponding $(N-1)$-mer; (3) a fully ordered prefibrillar species region where Q_w of the N-mer is equal to Q_w of the $(N-1)$-mer. The differences among these regions for the tetramers and the heptamers (Figure S4) suggest that the prefibrillar channel with disordered tips becomes more favorable as the oligomers grow.

We can define a disordered monomer as being a monomer whose number of interchain parallel hydrogen bonds is smaller than its number of interchain antiparallel hydrogen bonds. A disordered monomer forms a β-hairpin rather than the more fibril-like β-sheet. We constructed another free energy profile using the oligomer size and the number of individual disordered monomers as coordinates. Two regions are apparent and are shown divided by the black arrow: (1) a

https://doi.org/10.1021/acs.jpcb.2c03676
J. Phys. Chem. B XXXX, XXX, XXX−XXX

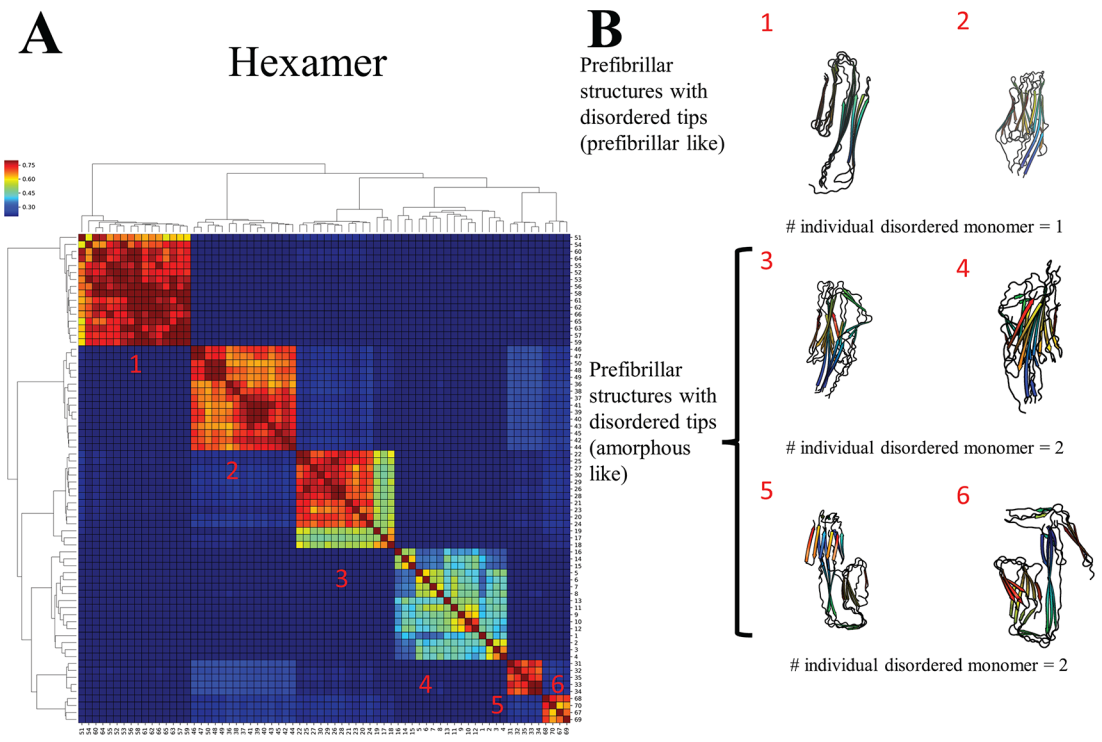

Figure 4. Cluster analysis of α-synuclein hexamers. (A) Cluster diagram of sampled hexamers using mutual Q. (B) Representative structures of the different clusters are shown: each monomer is colored by using a rainbow spectrum from red to blue, N-terminus to C-terminus.

disordered oligomeric species region where the more than half of the monomers are individually disordered; (2) a region corresponding to prefibrillar oligomers with disordered tips when less than half of the oligomers individually are disordered. From this landscape (Figure S5), the prefibrillar channel with disordered tip finally overwhelms the amorphous oligomeric states channel when the oligomer grows. The same trend is observed when considering the free energy profile by using as coordinates the number of interchain parallel hydrogen bonds and the number of interchain antiparallel hydrogen bonds of disordered monomers in oligomers (Figure S6).

Three basins are labeled as (1) disordered oligomeric states, (2) prefibrillar states with disordered tips, and (3) ordered prefibrillar states

3.4. Clustering the Prefibrillar Oligomers with Disordered Tips. In Figures 2, S1, and S2, we have already found that prefibrillar oligomers with disordered tips have more interchain parallel hydrogen bonds than fully disordered oligomers do but less than fully ordered prefibrillar oligomers have, suggesting the end monomer is a β hairpin. In Figure 4A, a cluster map of prefibrillar structures with disordered tips is constructed by using the mutual Q. Six significant clusters can be identified from the cluster analysis of the hexamer disordered tip structures. We have obtained the centroid structure for each cluster defined by its largest sum of the mutual Q values with all other structures in the corresponding cluster. These are shown in Figure 4B. Two kinds of prefibrillar structures with disordered tips can be identified by using the number of disordered monomers as a guide: (1) one class with disordered tips, which possess a single disordered monomer (clusters 1 and 2); (2) another set of amorphous-like prefibrillar structures which possess two individual disordered monomers (clusters 3, 4, 5, and 6). We also performed this cluster analysis of prefibrillar structures for the heptamer oligomers (Figure S6). The same two classes are also found, suggesting that the number of individual disordered monomers can be seen as a characteristic of the prominent feature of prefibrillar oligomers with disordered tips. We also show the structural differences between the prefibrillar species and the prefibrillar species having disordered tips in Figure S9

Furthermore, we have explored how the population of the different categories of structures varies using the number of individual disordered monomers to discriminate among them. On the basis of the finite size corrected free energy profiles for the different oligomer sizes (Figure 1B), we constructed 1D free energy profiles for the disordered tip channel by itself using the number of individual disordered monomers in Figure S7. Prefibrillar species with disordered tips are identified as those with less than half their monomers individually being disordered, while fully disordered oligomeric species are identified as those having more than half of their monomers individually disordered. For oligomers smaller than size six, more than three disordered monomers are typically incorporated, suggesting the dominance of the disordered oligomeric species (as we concluded in Figure 1A). When the oligomer size is larger than 6, prefibrillar species with disordered tips prefer to have two disordered monomers but generally do not have more than three disordered monomers in them (Figure 4). Disordered oligomeric species are not favorable once the oligomer size becomes larger than 6, supporting the dominance of the fibrillar channels upon growth.

3.5. Interplay between the Two Prefibrillar Channels. We have already found that the prefibrillar oligomers with disordered tips are more favorable than the fully disordered oligomers once the oligomers are large (Figure 1). The ordered prefibrillar channel is favorable during the whole aggregation process, but the barriers between the two

https://doi.org/10.1021/acs.jpcb.2c03676
J. Phys. Chem. B XXXX, XXX, XXX−XXX

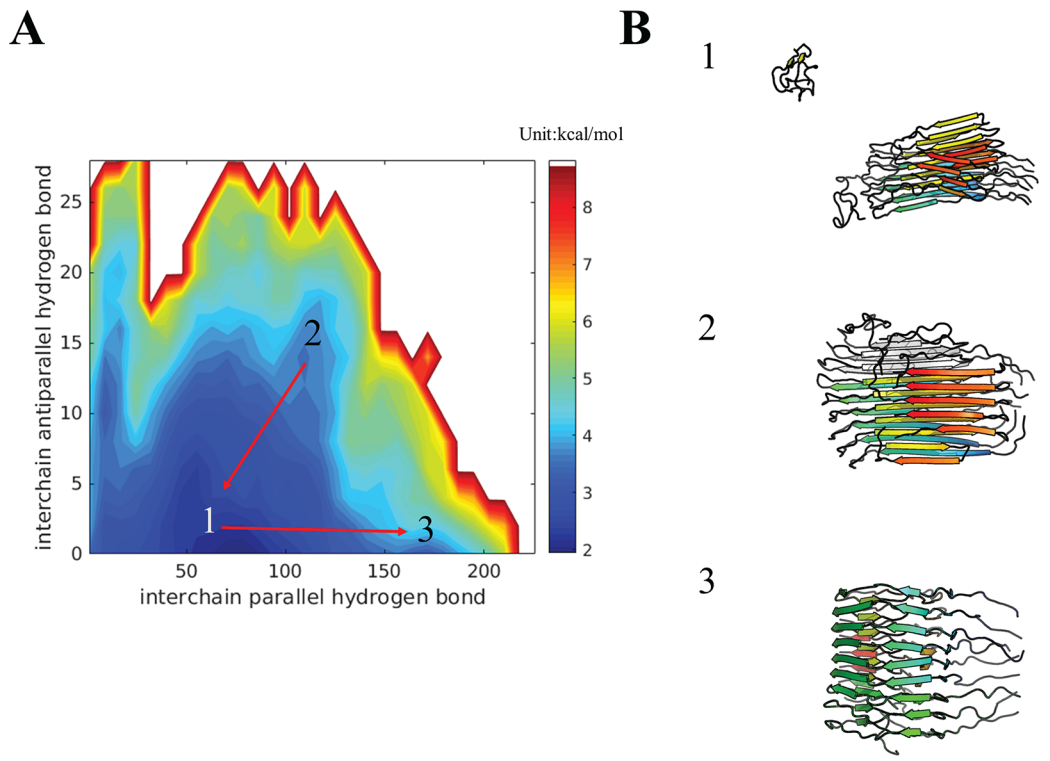

Figure 5. Grand canonical free energy profiles for α-synuclein at a temperature of 300 K. (A) The 2D free energy profile of 9-mer and 8-mer with a free monomer at the concentration of 133 μM is plotted by using the number of intermolecular parallel hydrogen bonds and the number of intramolecular antiparallel hydrogen bonds. (B) Representative structures for the different basins are shown: each monomer is colored with a rainbow spectrum from red to blue, N-terminus to C-terminus.

prefibrillar channels are not significantly larger than the barriers between oligomeric state as each of the two channels grows. The ordered prefibrillar species are energetically favored due to their structures, which possess more minimally frustrated interactions and fewer highly frustrated interactions than structures with disordered tips (Figure 2). We further explored the interplay between the two channels at large oligomer size. To directly sample the interconversion between the two channels, we performed another set of umbrella samplings starting from a fully ordered prefibrillar octamer along with a free monomer in a periodic box using the Q_{diff} between the ordered prefibrillar and the one of prefibrillar 9-mers with disordered tips found in the previous simulations. We constructed a two-dimensional free energy landscape using as coordinates the number of interchain parallel hydrogen bonds and the number of interchain antiparallel hydrogen bonds among all chains. As shown in Figure 5, three groups of species can be distinguished in the free energy surface: (1) an ordered prefibrillar octamer with a free monomer, (2) a prefibrillar 9-mer with disordered tips, and (3) a fully ordered prefibrillar 9-mer. Both the ordered prefibrillar species are more favorable than the prefibrillar oligomer having a disordered tip. At the same time, the barrier between the prefibrillar 9-mer with disordered tips and the ordered prefibrillar 9-mer is quite significant in comparison to the barriers between the ordered prefibrillar octamer with a free monomer and the other two species, suggesting there is some difficulty in carrying out directly an interconversion between prefibrillar species with disordered tips and the fully ordered prefibrillar species of the same oligomer size. The rearrangement of these species represents a kinetic barrier. The transition between the two channels is more easily made by first the dissociation of the end monomers which form a β-hairpin in the disordered tips structures followed by an ordered reassociation. In the simulations, we did not observe any direct transitions between the two channels at the same oligomer size. Instead, the dissociation and reassociation of the end monomers was frequently observed. These observations suggest a backtracking mechanism, which is in harmony with the stop-and-go mechanism that has been uncovered in experiments.[44] We see that the two nearly kinetically independent fibrillar growth channels occasionally can be connected through a backtracking event. Our observations suggest that the dissociation and reassociation of an end monomer to the prefibrillar core is the kinetically favored route in the aggregation process, consistent with the kinetic features found in experiments.[45,46]

3.6. Effect of Serine 87 Phosphorylation on α-Synuclein Aggregation. In Parkinson's disease, the aggregation of α-synuclein can be affected by several different post-translational modifications, including phosphorylation, mutation, ubiquitination, nitration, and truncation.[16−19] We can use statistical mechanical perturbation theory in AWSEM to study these effects focusing on phosphorylation.[17] The sites of α-synuclein that can be phosphorylated include one site (Figure 6B) in the hydrophobic NAC region and four sites in the acidic region.[19] The α-synuclein region studied in our simulations only incorporates a single phosphorylatable site (serine 87). The aggregation, however, can be a mixture in which the phosphorylated chains are chosen at random. We used the phosphorylation scheme described in the Methods section to account for the heterogeneity of phosphorylation. In vitro, multiple kinases, such as casein kinases,[47] GRKs (G protein-coupled receptor kinases),[48] LRRK2 (leucine-rich repeat kinase 2),[49] and PLKs (polo-like kinases),[50] have

https://doi.org/10.1021/acs.jpcb.2c03676
J. Phys. Chem. B XXXX, XXX, XXX−XXX

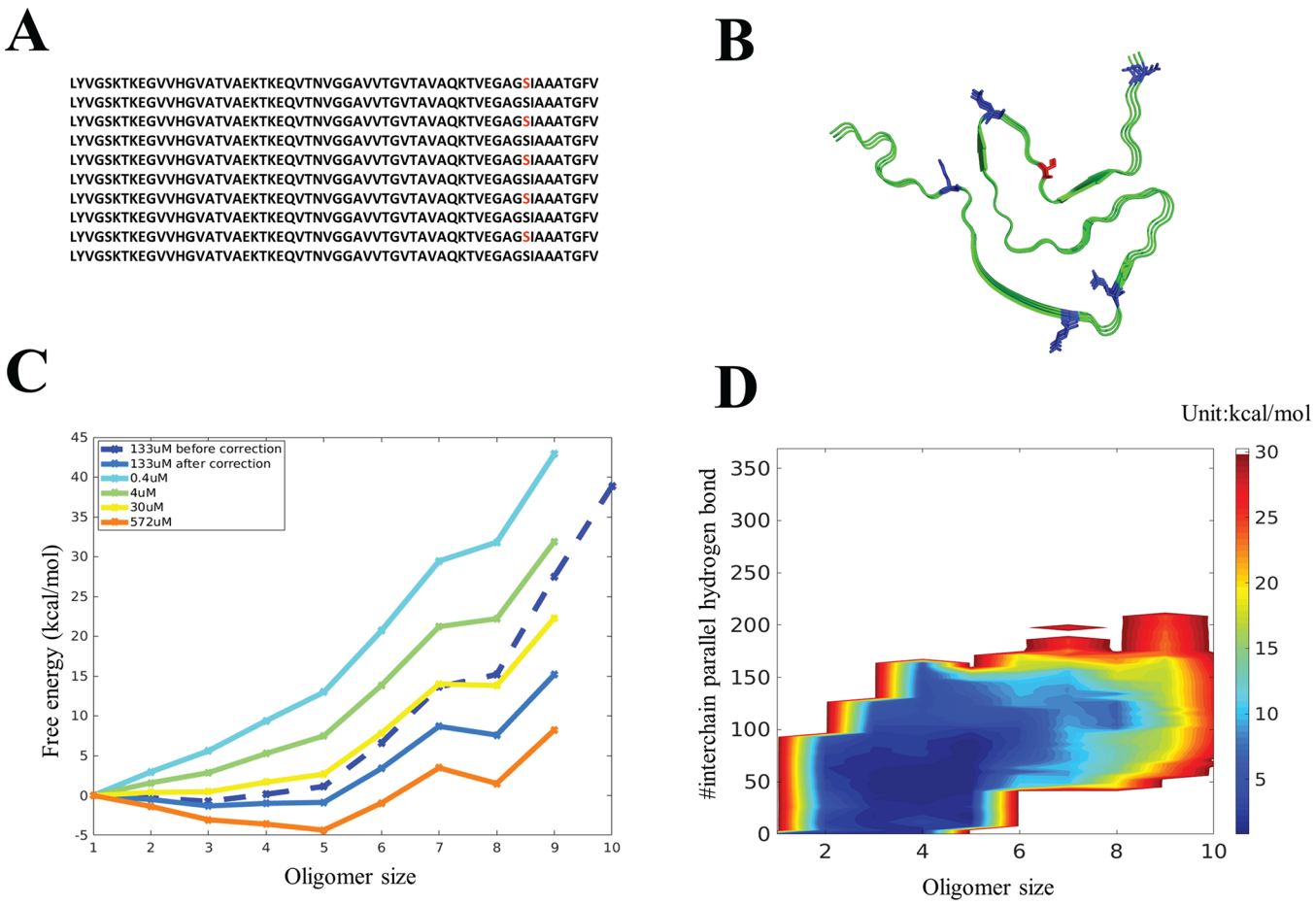

Figure 6. Effects of phosphorylation on the aggregation of α-synuclein. (A) Amino acid sequence of α-synuclein. The phosphorylated serine sites in perturbation are colored as red. (B) Solved fibrillar structure of α-synuclein is shown in cartoon. The negative residues are shown in stick form as blue, the positive residues are shown in stick form as yellow, and the phosphorylated residue are shown in stick form as red. (C) Perturbation-based grand canonical free energy profiles for different oligomer states as corrected for finite-size effects. (D) Perturbation-based free energy surface at the concentration of 133 μM at 300 K is plotted by using the number of interchain parallel hydrogen bonds and the oligomer size. Free energies are shown in rainbow colors (in units of kcal/mol).

been shown to be able to carry out the phosphorylation specifically for serine 129 and serine 87.[51] In vivo, the precise phosphorylated sites and the fraction of phosphorylated chains of α-synuclen doubtless depend on the interactions of a variety of kinases.[52]

We constructed the one-dimensional free energy profile of α-synuclein in its phosphorylated forms using perturbation theory and compared landscape with the nonphosphorylation profile in Figure 6C. The sequence used in our simulation includes only the NAC region so that it contains only a single phosphorylable site, serine 87. Phosphorylation of serine 87 makes fibril growth unfavored at the nominal laboratory concentration, suggesting that the α-synuclein aggregation can be inhibited by phosphorylating serine 87. Also, when the oligomers grow in size, the prefibrillar channels are also less favorable than they were for the nonphosphorylated versions in as seen Figure 6D. These results are supported by the laboratory report that phosphorylation of serine 87 indeed inhibits α-synuclein fibrillization.[19] In contrast with the instability of the prefibrillar channels at large oligomer size, the amorphous states remain still favored above the nominal laboratory concentration. These results imply that the phosphorylated serine 87 encourages the formation of small amorphous oligomers rather than fibrils or high-order oligomers.

4. CONCLUSION

Considering the complexity and richness of the aggregation process due to the diversity of the species involved, it has been hard to develop fully accurate kinetics models of protein aggregation and fibril elongation. Using dynamic light scattering (DLS) and Fourier transform infrared spectroscopy-(FTIR), Fink[53] and Iljina et al.[37] have found many of the species characterized in our simulation: amorphous aggregates, off-pathway oligomers, and fibrils during the aggregation. As seen in Figure 7, the disordered oligomeric states leading to amorphous aggregates and the ordered prefibrillar channel leading to fibrils turn out to be nearly kinetically independent, in agreement with the experimental evidence.[53] We propose that there should be a backtracking mechanism from the ordered prefibrillar states to the disordered oligomeric states because the barriers for interconversion between these states are larger than the barriers for the growth along a given channel. In the simulations, transitions between these channels are most easily made through dissociation and reassociation along the change of the oligomer size. Iljina and co-workers have found evidence for two different species when the

https://doi.org/10.1021/acs.jpcb.2c03676
J. Phys. Chem. B XXXX, XXX, XXX−XXX

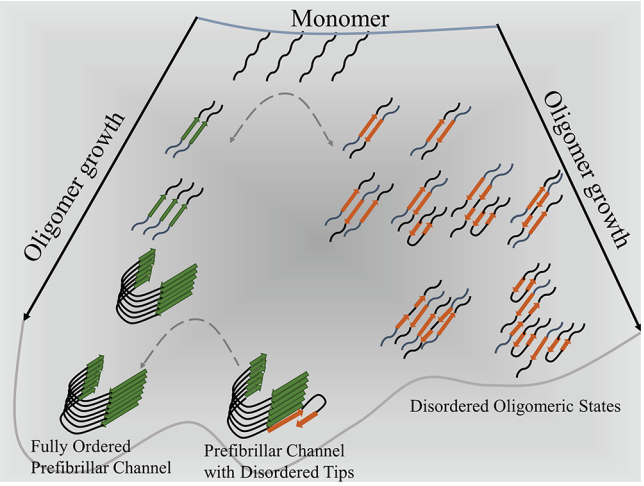

Figure 7. Schematic diagram of the growth of oligomers along the ordered prefibrillar channel and the disordered oligomeric states and the interconversion between different states. The prefibrillar-like chains and the amorphous-like chains are colored differently. Diverse species are shown to illustrate the interplay between the disordered oligomeric states, the prefibrillar channel with disordered tips, and the fully ordered prefibrillar channel.

oligomers are larger than **6** in size using fluorescence resonance energy transfer (FRET), supporting the coexistence of the ordered prefibrillar channel and the prefibrillar channel with disordered tips in our present theoretic works.[37] Considering the large barrier between two channels, the structural similarity between prefibrillar oligomers with disordered tips and fully ordered prefibrillar oligomers suggests the necessity of a backtracking mechanism between the two channels during oligomers growth. Different from the growth of fully disordered oligomeric states, the two prefibrillar channels are not kinetically completely independent because the prefibrillar species with disordered tips species ordinarily possess only one or two end monomers having a β-hairpin. We see, however, that the ordered prefibrillar oligomers can grow quite long before they transit to one with disordered tips and then may backtrack to the original prefibrillar oligomers (Figure 7). This suggests a molecular explanation of the stop-and-go mechanism proposed by Wördehoff et al. on the basis of experiment.[44]

Backtracking provides a route whereby a protein overcomes a topological barrier through partially unfolding during the folding process. This sort of mechanism occurs but is relatively uncommon for globular protein folding on funneled landscapes. Recently, we have seen that the backtracking mechanism is, however, a critical feature in several different protein aggregation systems. It occurs both for Aβ and for tau aggregation.[6,8] The distinctive nature[53] of the channels for synucleins suggests the backtracking will lead to a stop-and-go growth mechanism.[44] In contrast for Aβ, backtracking is primarily manifested and detectable in the change in rate with stability as probed by adding denaturants.[6,54] Backtracking mechanisms, while giving rise to different experimental manifestations, may be a universal feature of protein aggregation processes because aggregated protein structures have not been positions selected for in evolution in contrast to globular folding where the funnel landscape ensures mechanistic robustness and reliable structure formation

In this paper, we have only surveyed the mechanism underlying α-synuclein aggregation in free solution. In the cell, synuclein aggregates often interact with membranes. We plan to explore the membrane's role in the aggregation process in future work.

■ ASSOCIATED CONTENT

Supporting Information

The Supporting Information is available free of charge at https://pubs.acs.org/doi/10.1021/acs.jpcb.2c03676.

Additional simulations results which further support our conclusions in the main text (PDF)

■ AUTHOR INFORMATION

Corresponding Author

Peter G. Wolynes − *Center for Theoretical Biological Physics, Houston, Texas 77005, United States; Department of Chemistry, Rice University, Houston, Texas 77005, United States; Department of Bioengineering, Rice University, Houston, Texas 77005, United States;* orcid.org/0000-0001-7975-9287; Phone: (713)348-4101; Email: pwolynes@rice.edu

Authors

Xun Chen − *Center for Theoretical Biological Physics, Houston, Texas 77005, United States; Department of Chemistry, Rice University, Houston, Texas 77005, United States*

Mingchen Chen − *Department of Research and Development, neoX Biotech, Beijing 102206, China;* orcid.org/0000-0003-3916-7871

Complete contact information is available at: https://pubs.acs.org/10.1021/acs.jpcb.2c03676

Notes

The authors declare no competing financial interest.

■ ACKNOWLEDGMENTS

This work was funded by the Center for Theoretical Biological Physics, sponsored by NSF Grant PHY-2019745. Additionally, we recognize the D. R. Bullard Welch Chair at Rice University, Grant C-0016 (to P.G.W.). We thank the Data Analysis and Visualization Cyberinfrastructure funded by National Science Foundation Grant OCI-0959097.

■ REFERENCES

(1) Angelova, P. R.; Choi, M. L.; Berezhnov, A. V.; Horrocks, M. H.; Hughes, C. D.; De, S.; Rodrigues, M.; Yapom, R.; Little, D.; Dolt, K. S.; et al. Alpha synuclein aggregation drives ferroptosis: an interplay of iron, calcium and lipid peroxidation. *Cell Death & Differentiation* **2020**, *27*, 2781−2796.

(2) Malek, N.; Swallow, D.; Grosset, K.; Anichtchik, O.; Spillantini, M.; Grosset, D. Alpha-synuclein in peripheral tissues and body fluids as a biomarker for P arkinson's disease−a systematic review. *Acta Neurologica Scandinavica* **2014**, *130*, 59−72.

(3) George, S.; Brundin, P. Immunotherapy in Parkinson's disease: micromanaging alpha-synuclein aggregation. *Journal of Parkinson's Disease* **2015**, *5*, 413−424.

(4) Chavarría, C.; Rodríguez-Bottero, S.; Quijano, C.; Cassina, P.; Souza, J. M. Impact of monomeric, oligomeric and fibrillar alpha-synuclein on astrocyte reactivity and toxicity to neurons. *Biochem. J.* **2018**, *475*, 3153−3169.

(5) Chen, M.; Wolynes, P. G. Aggregation landscapes of Huntingtin exon 1 protein fragments and the critical repeat length for the onset of

Huntington's disease. *Proc. Natl. Acad. Sci. U. S. A.* **2017**, *114*, 4406−4411.
(6) Zheng, W.; Tsai, M.-Y.; Chen, M.; Wolynes, P. G. Exploring the aggregation free energy landscape of the amyloid-β protein (1−40). *Proc. Natl. Acad. Sci. U. S. A.* **2016**, *113*, 11835−11840.
(7) Chen, M.; Tsai, M.; Zheng, W.; Wolynes, P. G. The aggregation free energy landscapes of polyglutamine repeats. *J. Am. Chem. Soc.* **2016**, *138*, 15197−15203.
(8) Chen, X.; Chen, M.; Schafer, N. P.; Wolynes, P. G. Exploring the interplay between fibrillization and amorphous aggregation channels on the energy landscapes of tau repeat isoforms. *Proc. Natl. Acad. Sci. U. S. A.* **2020**, *117*, 4125−4130.
(9) Goedert, M. Alpha-synuclein and neurodegenerative diseases. *Nat. Rev. Neurosci.* **2001**, *2*, 492−501.
(10) Bungeroth, M.; Appenzeller, S.; Regulin, A.; Völker, W.; Lorenzen, I.; Grötzinger, J.; Pendziwiat, M.; Kuhlenbäumer, G. Differential aggregation properties of alpha-synuclein isoforms. *Neurobiology of aging* **2014**, *35*, 1913−1919.
(11) Mochizuki, H.; Choong, C.-J.; Masliah, E. A refined concept: α-synuclein dysregulation disease. *Neurochemistry international* **2018**, *119*, 84−96.
(12) Anderson, V. L.; Ramlall, T. F.; Rospigliosi, C. C.; Webb, W. W.; Eliezer, D. Identification of a helical intermediate in trifluoroethanol-induced alpha-synuclein aggregation. *Proc. Natl. Acad. Sci. U. S. A.* **2010**, *107*, 18850−18855.
(13) Li, B.; Ge, P.; Murray, K. A.; Sheth, P.; Zhang, M.; Nair, G.; Sawaya, M. R.; Shin, W. S.; Boyer, D. R.; Ye, S.; et al. Cryo-EM of full-length α-synuclein reveals fibril polymorphs with a common structural kernel. *Nat. Commun.* **2018**, *9*, 1−10.
(14) Guerrero-Ferreira, R.; Taylor, N. M.; Mona, D.; Ringler, P.; Lauer, M. E.; Riek, R.; Britschgi, M.; Stahlberg, H. Cryo-EM structure of alpha-synuclein fibrils. *elife* **2018**, *7*, No. e36402.
(15) Fitzpatrick, A. W.; Falcon, B.; He, S.; Murzin, A. G.; Murshudov, G.; Garringer, H. J.; Crowther, R. A.; Ghetti, B.; Goedert, M.; Scheres, S. H. Cryo-EM structures of tau filaments from Alzheimer's disease. *Nature* **2017**, *547*, 185−190.
(16) Barrett, P. J.; Greenamyre, J. T. Post-translational modification of α-synuclein in Parkinson's disease. *Brain Research* **2015**, *1628*, 247−253.
(17) He, Y.; Yu, Z.; Chen, S. Alpha-synuclein nitration and its implications in Parkinson's disease. *ACS chemical neuroscience* **2019**, *10*, 777−782.
(18) Chen, L.; Periquet, M.; Wang, X.; Negro, A.; McLean, P. J.; Hyman, B. T.; Feany, M. B.; et al. Tyrosine and serine phosphorylation of α-synuclein have opposing effects on neurotoxicity and soluble oligomer formation. *J. Clin. Invest.* **2009**, *119*, 3257−3265.
(19) Paleologou, K. E.; Oueslati, A.; Shakked, G.; Rospigliosi, C. C.; Kim, H.-Y.; Lamberto, G. R.; Fernandez, C. O.; Schmid, A.; Chegini, F.; Gai, W. P.; et al. Phosphorylation at S87 is enhanced in synucleinopathies, inhibits α-synuclein oligomerization, and influences synuclein-membrane interactions. *J. Neurosci.* **2010**, *30*, 3184−3198.
(20) Nübling, G. S.; Levin, J.; Bader, B.; Lorenzl, S.; Hillmer, A.; Högen, T.; Kamp, F.; Giese, A. Modelling Ser129 phosphorylation inhibits membrane binding of pore-forming alpha-synuclein oligomers. *PLoS One* **2014**, *9*, No. e98906.
(21) Majbour, N. K.; Vaikath, N. N.; van Dijk, K. D.; Ardah, M. T.; Varghese, S.; Vesterager, L. B.; Montezinho, L. P.; Poole, S.; Safieh-Garabedian, B.; Tokuda, T.; et al. Oligomeric and phosphorylated alpha-synuclein as potential CSF biomarkers for Parkinson's disease. *Molecular neurodegeneration* **2016**, *11*, 1−15.
(22) Oueslati, A. Implication of alpha-synuclein phosphorylation at S129 in synucleinopathies: what have we learned in the last decade? *Journal of Parkinson's disease* **2016**, *6*, 39−51.
(23) Davtyan, A.; Schafer, N. P.; Zheng, W.; Clementi, C.; Wolynes, P. G.; Papoian, G. A. AWSEM-MD: protein structure prediction using coarse-grained physical potentials and bioinformatically based local structure biasing. *J. Phys. Chem. B* **2012**, *116*, 8494−8503.
(24) Jin, S.; Contessoto, V. G.; Chen, M.; Schafer, N. P.; Lu, W.; Chen, X.; Bueno, C.; Hajitaheri, A.; Sirovetz, B. J.; Davtyan, A.; et al. AWSEM-Suite: a protein structure prediction server based on template-guided, coevolutionary-enhanced optimized folding landscapes. *Nucleic acids research* **2020**, *48*, W25−W30.
(25) Zheng, W.; Schafer, N. P.; Davtyan, A.; Papoian, G. A.; Wolynes, P. G. Predictive energy landscapes for protein−protein association. *Proc. Natl. Acad. Sci. U. S. A.* **2012**, *109*, 19244−19249.
(26) Tsai, M.-Y.; Zhang, B.; Zheng, W.; Wolynes, P. G. Molecular mechanism of facilitated dissociation of Fis protein from DNA. *J. Am. Chem. Soc.* **2016**, *138*, 13497−13500.
(27) Cho, S. S.; Levy, Y.; Wolynes, P. G. P versus Q: Structural reaction coordinates capture protein folding on smooth landscapes. *Proc. Natl. Acad. Sci. U. S. A.* **2006**, *103*, 586−591.
(28) Chen, M.; Schafer, N. P.; Zheng, W.; Wolynes, P. G. The AWSEM-Amylometer: predicting amyloid propensity and fibril topology using an optimized folding landscape model. *ACS Chem. Neurosci.* **2018**, *9*, 1027−1039.
(29) Shen, T.; Zong, C.; Hamelberg, D.; Andrew Mccammon, J.; Wolynes, P. G. The folding energy landscape and phosphorylation: modeling the conformational switch of the NFAT regulatory domain. *FASEB J.* **2005**, *19*, 1389−1395.
(30) Lätzer, J.; Shen, T.; Wolynes, P. G. Conformational switching upon phosphorylation: a predictive framework based on energy landscape principles. *Biochemistry* **2008**, *47*, 2110−2122.
(31) Ferreiro, D. U.; Hegler, J. A.; Komives, E. A.; Wolynes, P. G. Localizing frustration in native proteins and protein assemblies. *Proc. Natl. Acad. Sci. U. S. A.* **2007**, *104*, 19819−19824.
(32) Chen, M.; Chen, X.; Schafer, N. P.; Clementi, C.; Komives, E. A.; Ferreiro, D. U.; Wolynes, P. G. Surveying biomolecular frustration at atomic resolution. *Nat. Commun.* **2020**, *11*, 1−9.
(33) Chen, M.; Chen, X.; Jin, S.; Lu, W.; Lin, X.; Wolynes, P. G. Protein Structure Refinement Guided by Atomic Packing Frustration Analysis. *J. Phys. Chem. B* **2020**, *124*, 10889−10898.
(34) Ferreiro, D. U.; Hegler, J. A.; Komives, E. A.; Wolynes, P. G. On the role of frustration in the energy landscapes of allosteric proteins. *Proc. Natl. Acad. Sci. U. S. A.* **2011**, *108*, 3499−3503.
(35) Chen, M.; Schafer, N. P.; Wolynes, P. G. Surveying the energy landscapes of Aβ fibril polymorphism. *J. Phys. Chem. B* **2018**, *122*, 11414−11430.
(36) Xu, Y.; Knapp, K.; Le, K. N.; Schafer, N. P.; Safari, M. S.; Davtyan, A.; Wolynes, P. G.; Vekilov, P. G. Frustrated peptide chains at the fibril tip control the kinetics of growth of amyloid-β fibrils. *Proc. Natl. Acad. Sci. U. S. A.* **2021**, *118*, e2110995118 DOI: 10.1073/pnas.2110995118.
(37) Iljina, M.; Garcia, G. A.; Horrocks, M. H.; Tosatto, L.; Choi, M. L.; Ganzinger, K. A.; Abramov, A. Y.; Gandhi, S.; Wood, N. W.; Cremades, N.; et al. Kinetic model of the aggregation of alpha-synuclein provides insights into prion-like spreading. *Proc. Natl. Acad. Sci. U. S. A.* **2016**, *113*, E1206−E1215.
(38) Cremades, N.; Cohen, S. I.; Deas, E.; Abramov, A. Y.; Chen, A. Y.; Orte, A.; Sandal, M.; Clarke, R. W.; Dunne, P.; Aprile, F. A.; et al. Direct observation of the interconversion of normal and toxic forms of α-synuclein. *Cell* **2012**, *149*, 1048−1059.
(39) Reiss, H.; Bowles, R. K. Some fundamental statistical mechanical relations concerning physical clusters of interest to nucleation theory. *J. Chem. Phys.* **1999**, *111*, 7501−7504.
(40) Afitska, K.; Fucikova, A.; Shvadchak, V. V.; Yushchenko, D. A. α-Synuclein aggregation at low concentrations. *Biochimica et Biophysica Acta (BBA)-Proteins and Proteomics* **2019**, *1867*, 701−709.
(41) Krishnan, S.; Chi, E. Y.; Wood, S. J.; Kendrick, B. S.; Li, C.; Garzon-Rodriguez, W.; Wypych, J.; Randolph, T. W.; Narhi, L. O.; Biere, A. L.; et al. Oxidative dimer formation is the critical rate-limiting step for Parkinson's disease α-synuclein fibrillogenesis. *Biochemistry* **2003**, *42*, 829−837.
(42) Narkiewicz, J.; Giachin, G.; Legname, G. In vitro aggregation assays for the characterization of α-synuclein prion-like properties. *Prion* **2014**, *8*, 19−32.

https://doi.org/10.1021/acs.jpcb.2c03676
J. Phys. Chem. B XXXX, XXX, XXX−XXX

(43) Powers, E. T.; Powers, D. L. The kinetics of nucleated polymerizations at high concentrations: amyloid fibril formation near and above the "supercritical concentration". *Biophys. J.* **2006**, *91*, 122−132.
(44) Wördehoff, M. M.; Bannach, O.; Shaykhalishahi, H.; Kulawik, A.; Schiefer, S.; Willbold, D.; Hoyer, W.; Birkmann, E. Single fibril growth kinetics of α-synuclein. *J. Mol. Biol.* **2015**, *427*, 1428−1435.
(45) Lorenzen, N.; Nielsen, S. B.; Buell, A. K.; Kaspersen, J. D.; Arosio, P.; Vad, B. S.; Paslawski, W.; Christiansen, G.; Valnickova-Hansen, Z.; Andreasen, M.; et al. The role of stable α-synuclein oligomers in the molecular events underlying amyloid formation. *J. Am. Chem. Soc.* **2014**, *136*, 3859−3868.
(46) Buell, A. K.; Galvagnion, C.; Gaspar, R.; Sparr, E.; Vendruscolo, M.; Knowles, T. P.; Linse, S.; Dobson, C. M. Solution conditions determine the relative importance of nucleation and growth processes in α-synuclein aggregation. *Proc. Natl. Acad. Sci. U. S. A.* **2014**, *111*, 7671−7676.
(47) Waxman, E. A.; Giasson, B. I. Specificity and regulation of casein kinase-mediated phosphorylation of α-synuclein. *Journal of Neuropathology & Experimental Neurology* **2008**, *67*, 402−416.
(48) Gonçalves, S.; Outeiro, T. F. Assessing the subcellular dynamics of alpha-synuclein using photoactivation microscopy. *Molecular neurobiology* **2013**, *47*, 1081−1092.
(49) Qing, H.; Wong, W.; McGeer, E. G.; McGeer, P. L. Lrrk2 phosphorylates alpha synuclein at serine 129: Parkinson disease implications. *Biochemical and biophysical research communications* **2009**, *387*, 149−152.
(50) Beyer, K.; Ariza, A. alpha-Synuclein posttranslational modification and alternative splicing as a trigger for neurodegeneration. *Molecular neurobiology* **2013**, *47*, 509−524.
(51) Kosten, J.; Binolfi, A.; Stuiver, M.; Verzini, S.; Theillet, F.-X.; Bekei, B.; van Rossum, M.; Selenko, P. Efficient modification of alpha-synuclein serine 129 by protein kinase CK1 requires phosphorylation of tyrosine 125 as a priming event. *ACS chemical neuroscience* **2014**, *5*, 1203−1208.
(52) Weston, L. J.; Cook, Z. T.; Stackhouse, T. L.; Sal, M. K.; Schultz, B. I.; Tobias, Z. J.C.; Osterberg, V. R.; Brockway, N. L.; Pizano, S.; Glover, G.; Weissman, T. A.; Unni, V. K. In vivo aggregation of presynaptic alpha-synuclein is not influenced by its phosphorylation at serine-129. *Neurobiology of Disease* **2021**, *152*, 105291−105291.
(53) Fink, A. L. The aggregation and fibrillation of α-synuclein. *Acc. Chem. Res.* **2006**, *39*, 628−634.
(54) Lee, S.; Fernandez, E. J.; Good, T. A. Role of aggregation conditions in structure, stability, and toxicity of intermediates in the Aβ fibril formation pathway. *Protein Sci.* **2007**, *16*, 723−732.

https://doi.org/10.1021/acs.jpcb.2c03676
J. Phys. Chem. B XXXX, XXX, XXX−XXX